Available online at www.sciencedirect.com

ScienceDirect

Energy Procedia 77 (2015) 487 – 492

Energy Procedia

5th International Conference on Silicon Photovoltaics, SiliconPV 2015

Properties of liquid phase crystallized interdigitated back-contact solar cells on glass

Paul Sonntag[1], Jan Haschke[1], Sven Kühnapfel[1], Onno Gabriel[2], Daniel Amkreutz[1], Bernd Rech[1]

[1]*Helmholtz Zentrum Berlin für Materialien und Energie GmbH, Kekuléstr.5, 12489 Berlin, Germany*
[2]*PVcomB/Helmholtz-Zentrum Berlin für Materialien und Energie GmbH, Schwarzschildstr. 3,12489 Berlin, Germany*

Abstract

We fabricated interdigitated back-contact silicon hetero-junction solar cells based on thin-film absorbers on glass. The Si absorbers were directly deposited on the glass and crystallized using liquid phase crystallization. To compare whether our contact system is applicable to a wide range of initial absorber conditions two different types of precursors were prepared with absorber thicknesses between 2.5-9 µm. Furthermore, glass superstrates, doping densities and interlayer stacks were varied. With a KOH random pyramid light trapping texture at the back more than 30 mA/cm² were achieved on an electron beam evaporated precursor material and 655 mV on a PECVD precursor material.

Peer review by the scientific conference committee of SiliconPV 2015 under responsibility of PSE AG

Keywords: Liquid Phase Crystallization, IBC, silicon hetero-juntion, thin-film crystalline silicon solar cell

1. Introduction

The silicon photovoltaics market is under constant pressure to reduce costs and minimize material consumption by decreasing absorber thicknesses. Conventional wafer technology is not an appropriate technology to go to absorber thicknesses below 50 µm, due to unavoidable kerf losses and handling problems during fabrication. Liquid phase crystallization (LPC) of amorphous or nano-crystalline thin silicon layers directly on glass offers a way to combine both the possibility to fabricate any desired absorber thickness between 5-40 µm and possibility to avoid sawing losses, while the glass itself provides mechanical stability. A line-shaped energy source (continuous wave (cw) laser or electron beam) is scanned across the amorphous or nano-crystalline surface to locally melt the silicon such that it crystallizes along the scanning direction forming multi-crystalline silicon with grain sizes of up to few

Peer review by the scientific conference committee of SiliconPV 2015 under responsibility of PSE AG
doi:10.1016/j.egypro.2015.07.069

millimeters in width and up to centimeters in length. Open circuit voltages of up to 656 mV are feasible on highly doped absorbers (N_D=2*10^{18}/cm³) [1] and a good absorber quality was shown [2]. Since the crystallized silicon cannot be contacted from the glass-side, contact systems for this type of absorbers are always single-sided [3, 4]. High temperature processes would deform or damage the glass, consequently a silicon hetero-junction (SHJ) comprising amorphous hydrogenated silicon layers is suitable for contacting. In this work we present latest cell results of the **H**etero- **I**nterdigitated Back-Contacts on **P**oly-**S**ilicon **T**hin-Film Absorb**ER** (HIPSTER) system presented in a publication submitted to Prog. Photovolt: Res. Appl. in Feb. 2015 (accepted Jun. 2015). An IBC-SHJ contact system combines the advantages of high j_{SC} potential due to the absence of front shadowing and high V_{OC} potential resulting from the hetero-junction [5, 6].

The cells discussed in this work show that the realization of an IBC-SHJ system for LPC Si on glass works on different Si precursor materials and glass superstrates over a range of doping densities and absorber thicknesses.

2. Cell fabrication

To compare a set of different initial conditions on cell performance, two vastly different types were fabricated (from now on denoted Cell A and B). Cell A was processed on Corning Eagle XG glass, whereas for Cell B Schott Borofloat 33 glass. Interlayers serving as ARC, glass contaminant diffusion barrier, wetting promoter and front side passivation consisted of a reactively sputtered stack of $SiO_x/SiN_x/SiO_x$ (250/70/20) nm [7] and $SiN_x/SiO_x/SiN_x/SiO_xN_y$ (10/200/60/20) nm deposited by PECVD [8] for Cell A and B, respectively. The precursor Si absorber material was applied either by electron beam evaporation (Cell A) or PECVD (Cell B). Subsequently, Cell A was liquid phase crystallized using an electron beam in vacuum, with a SiO_x cap to promote wetting [9], whereas Cell B was liquid phase crystallized using a cw line shaped laser by LIMO under ambient conditions without a SiO_x cap. A summary of those differences is found in table 1.

Table 1. HIPSTER Cells processed for this work.

	Cell A	Cell B
Glass superstrate	Corning Eagle XG	Schott Borofloat 33
Interlayer stack	SiOx/SiNx/SiOx (250/70/20) nm by reactive sputtering	SiNx/SiOx/SiNx/SiOxNy (10/200/60/20) nm by PECVD
Precursor Si material	Electron beam evaporation	PECVD
Crystallization method	Electron Beam, vacuum, SiOx cap	cw laser, ambient, no cap
Final absorber thickness	~ 9 µm	~ 2.5 µm

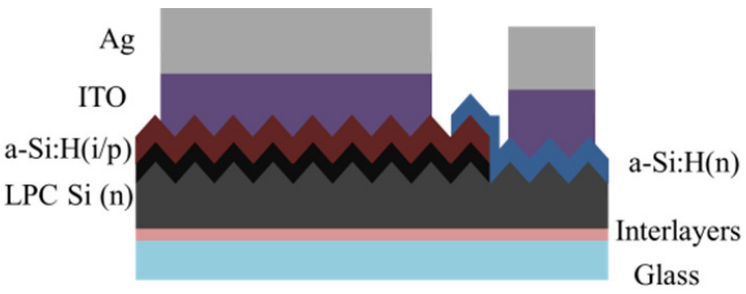

Fig. 1. Schematic cross section of the IBC-SHJ system on glass.

Afterwards, both cells were textured with random pyramids using a KOH solution. The same contact system using identical parameters was processed on both Cell A and B. Details of the fabrication will be found in a publication submitted to Prog. Photovolt: Res. Appl. Feb. 2015. In summary, it is built using two photolithography steps to structure a-Si:H(i/p) as minority charge carrier contact and a-Si:H(n) as majority contact, both deposited using PECVD, into an interdigitating comb pattern. In the a-Si:H(n) patterning step

diluted NaOH is used as selective etchant. It has an about 30 times lower etch rate on p-type amorphous silicon than on n-type. This way one can assure to remove the n-type completely by choosing appropriate etching times. Finally, a third photolithography step defines the beforehand sputtered ITO/Ag electrodes. The complete setup is displayed in Fig. 1. An overlap between a-Si:H(n) and (p) takes care that the absorber is completely passivated. Finally, an annealing step is necessary to crystallize ITO, which was deposited at room temperature [10]. To this end, the cells are placed on a hotplate at 200°C for 30 min.

3. Experimental

J-V-characteristics were recorded using a sun simulator by Wacom WXS-156S - L2, AM1.5GMM, with dual sources (tungsten and xenon lamp) and class AAA characteristics at a temperature of 25°C. Suns-V_{OC} curves were recorded using a setup by Sinton. Quantum efficiencies (QE) were determined in a self-constructed setup using a spot size of 3x2 mm. Optical simulations were done with Wafer Ray Tracer (version 1.4.3) [19]. Hall measurements were conducted using an Ecopia HMS-3000 Hall Measurement System by Bridge Technology. UV/VIS reflectivity and absorption sprectra were recorded using a Lambda 1050 setup by Perkin Elmer.

4. Results

The j-V-characteristics of cell A and B were measured (Fig. 2 (a)), with an anti-reflection foil by DSM advanced surfaces (ARF) on the glass to enhance light incoupling (solid lines) and by Suns-V_{OC} (dashed lines). Table 2 summarizes the key parameters. On both absorber-superstrate systems a V_{OC} well above 600 mV was achieved. The on average 2.5 µm thin absorber of Cell B yielded a j_{SC} of 23.5 mA/cm², whereas the thicker absorber of Cell B yielded 30.3 mA/cm². The j_{SC} are confirmed by external quantum efficiency (EQE) measurements seen in Fig. 2 (b). The integrated spectral response results in a j_{SC} of 28.1 and 25.4 mA/cm² for Cell A and B, respectively. To investigate series resistance influences, Suns-V_{OC} measurements of both cells were also recorded (Fig. 2 (a)). The pseudo FF of the Suns-V_{OC} curves is 12%$_{abs}$ and 25%$_{abs}$ higher than the one determined from the solar simulator curve for Cell A and B, respectively. Internal quantum efficiency (IQE) was determined by dividing the EQE by (1-R-T); where R is the reflectivity and T the transmission of the cell, measured with a UV/VIS spectrometer. A wide plateau of over 83 % from 400 nm – 840 nm was recorded for Cell A with a peak value of 88 % and an IQE peak value of 81 % at 520 nm with a slight descend towards higher wavelengths for Cell B.

SEM images (Fig. 3) were taken of the cross section of the absorber of both cells to determine the layer thickness of the absorbers after all surface etching treatments including the KOH random pyramid texture. Since KOH anisotropically etches silicon [11], a different surface pattern is observed for different grain orientations. It ranges from completely upright pyramids as seen in Fig. 3 (a) and (c) on Cell A and B, respectively, where the initial grain orientation was close to <100>, to tilted (d) and almost lying pyramids (b) with grain orientations approaching <111> initial orientation. As a consequence of the anisotropic etching, absorber thicknesses range from 7.5 to 10 µm for Cell A and from 1.3 to 3 µm for Cell B.

Doping densities were measured on 5x5 mm test structures cut out of the same absorber as the cells to $3.7*10^{16}$/cm³ and $1.0*10^{17}$/cm³ for Cell A and B, respectively.

Table 2. HIPSTER Cells results.

	Cell A	Cell B
V_{OC} [mV]	612	655
j_{SC} [mA/cm²]	30.3	23.5
FF/pFF [%]	57	55
ETA [%]	10.5	8.5
pFF (derived from Suns-V_{OC}) [%]	69	80
Doping concentration N_D [1/cm³]	$3.7*10^{16}$	$1.0*10^{17}$

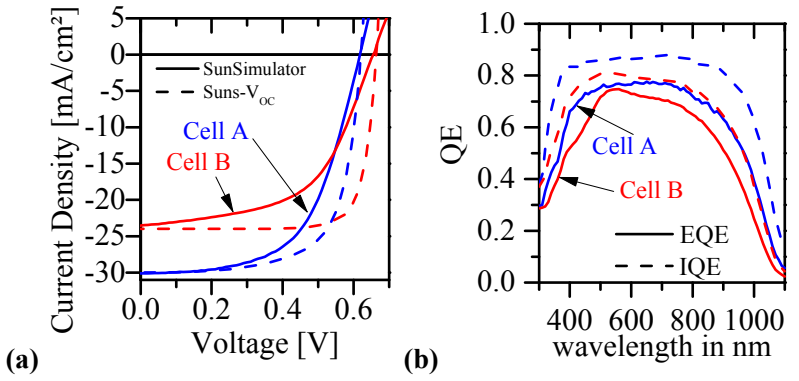

Fig. 2. (a) j-V-characteristics of Cell A (blue) and B (red) recorded with a sun simulator (solid) and by Suns-V_{OC} (dashed); (b) External (solid) and internal (dashed) quantum efficiencies of Cell A (blue) and B (red).

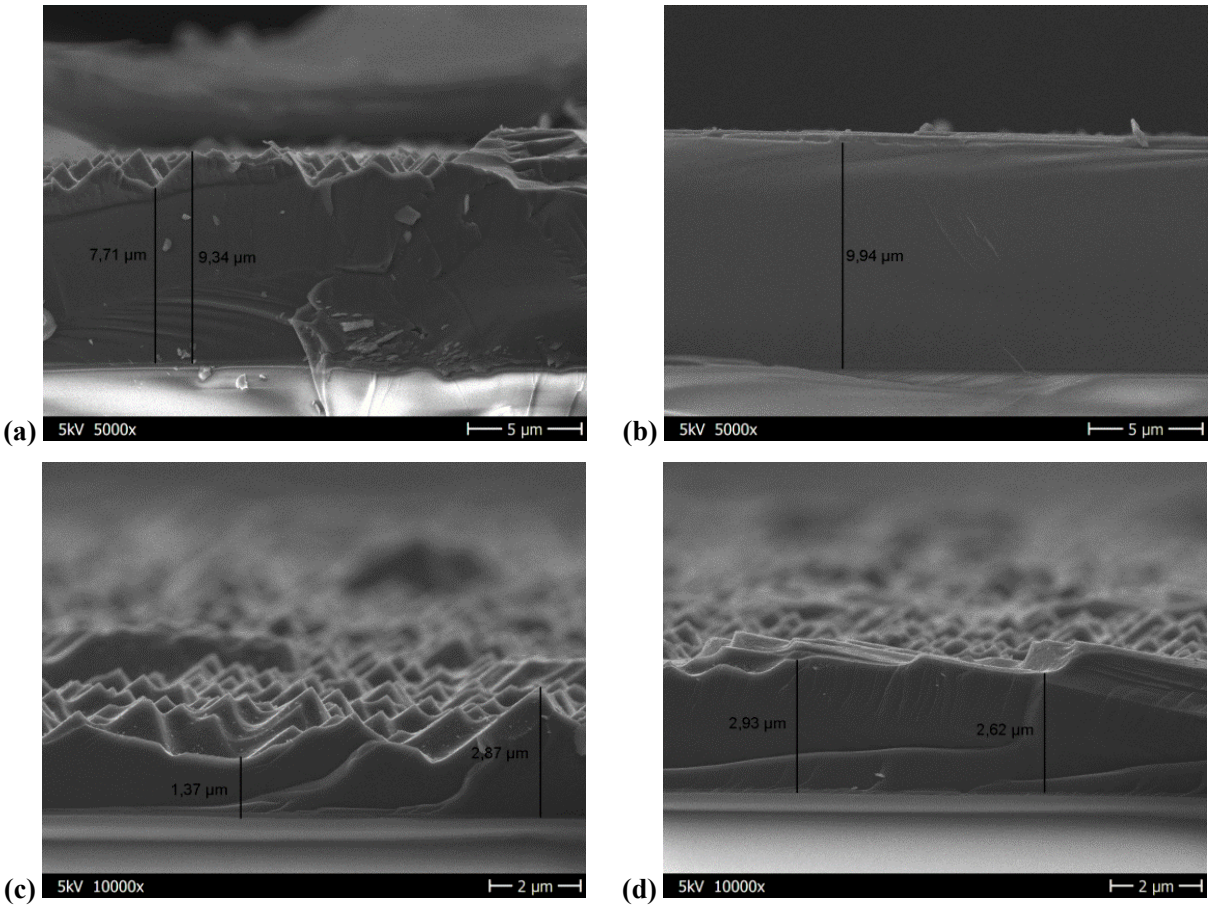

Fig. 3. SEM images of a cross section of the absorber for Cell A (a) and (b) and Cell B (c) and (d). (a) Position at the absorber with upright pyramids; (b) extremely tilted pyramids; (c) upright; (d) moderately tilted.

5. Discussion

Both Cell A and Cell B show a low FF, that can partly be attributed to shunt and series resistances. To further investigate possible losses in the cells, the pFF of the Suns-V_{OC} curve is one possible measure for the quality of the contact system and the material. Since for Cell A it is still below 70 %, in addition to resistance losses, problems with recombination in the junction, at the interfaces or at the grain boundaries are possible explanations for low real FF. Cell B on the contrary, shows a high pFF of 80 %, but also a high distributed series resistance. The latter can be seen by comparing the slope in the j-V-curve with the slope in the Suns-V_{OC} curve at lower voltages. The 80 % pFF would actually indicate a good absorber quality. However, this is not reflected in the IQE which is also a measure for the material, by ruling out any optical influences on the collection probability. It stays below 80 % for most of the spectrum. This indicates that also Cell B suffers from recombination losses as Cell A and that these losses are independent of the different initial absorber preparations used (cp. Table 1). Optimization of contact resistances and a-Si:H layers might be one possible way to mitigate the problem of low FF.

A high surface recombination in case of Cell B seems unlikely as a cause to reduce the FF since it would also affect the V_{OC}. However, a V_{OC} of 655 mV on an absorber doped $1.0*10^{17}/cm^3$ is quite high. The V_{OC} of 612 mV of Cell A in contrast to the 655 mV of Cell B is not completely clear. It could be explained by its lower doping concentration of $3.7*10^{16}/cm^3$, the different front passivation stack, its thickness being more than 3 times more, or a combination of all the above. The difference in j_{SC} between the two cells is 6.8 mA/cm². To check whether the difference in absorber thickness alone could be the cause of the higher j_{SC} in Cell A, simulations were conducted using Wafer Ray Tracer (version 1.4.3) [12]. Since the absorber thickness is inhomogeneous throughout the absorber (cp. Fig. 3) only an upper and lower estimate for the difference in j_{SC} can be calculated. In some parts of the cell, the initial grain orientation was close to <100> resulting in upright pyramids, and in other close to <111> resulting in an almost planar rear. Thus, simulations were conducted comparing two planar absorbers with thicknesses equal to almost planar regions of Cell A and B and two completely textured versions with pyramids having a base width of 2 µm and a height of 1.5 µm determined from SEM images shown in Fig. 3. The two completely planar simulated versions of the absorbers of Cell A and B yielded a j_{SC} difference of 7.4 mA/cm² determined from absorption spectra of AM1.5 incidence. Assuming the absorbers of the two Cells A and B had 100 % upright random pyramids, a difference of 2.9 mA/cm² was calculated. It is consequently possible that the difference in measured j_{SC} of 6.8 mA/cm² stems from the difference in absorber thickness, since the real texturing quality must also lie somewhere in the middle. The difference in measured j_{SC} to maximum possible j_{SC} according to the simulations would be a nice figure of merit for the area fraction of initially <100> oriented grains. However, it cannot be applied, since on the one hand the fraction of <100> grains might not be the same for both cells and on the other hand too many other parameters influence this value. Firstly, different glasses and interlayers were used, and secondly the doping density differed by almost one order of magnitude, which was not taken into account in the purely optic simulations. Nevertheless, the difference in j_{SC} for entirely planar and completely textured cells shows the importance of light trapping for thin-film devices.

6. Summary

In conclusion we fabricated IBC-SHJ solar cells using LPC Si on glass. To determine which range of initial conditions and deposition variations work for our contact scheme, two cells were fabricated with a wide variation in parameters. Although the two cells were made from different precursor Si materials on different glass substrates, with different doping densities and thicknesses, V_{OC} of over 610 mV was reached on both. A higher doping density of $1*10^{17}$ /cm³ led to a V_{OC} on the finished cell device of 655 mV with a current of 23.5 mA/cm² although the absorber thickness was less than 3 µm. On the 9 µm thick absorber, above 30 mA/cm² were achieved. This clearly demonstrates the potential of LPC Si and the IBC-SHJ contact system. However, FF remain below 70 % and inhibit higher cell efficiencies. Further investigations will focus on reducing series and increasing shunt resistances and a detailed examination of the absorber properties and possible limitations.

Acknowledgements

The authors would like to thank Martin Reiche, Kerstin Jacob, Mona Wittig, Mathias Mews, Erhard Conrad, Carola Klimm, Karolina Mack, Andreas Opitz, Holger Rhein, Manuel Hartig, Tim Frijnts and Tobias Hänel for experimental and analytical support. We thank DSM Advanced Surfaces for providing the textured light trapping anti reflection foil.

References

[1] Haschke J, Amkreutz D, Korte L, Ruske F, and Rech B. Towards wafer quality crystalline silicon thin-film solar cells on glass, Sol Energy Mater Sol Cells 2014; 128:190–197.

[2] Haschke J, Amkreutz D, Frijnts T, Hänel T, and Rech B. Influence of Barrier and Doping Type on the Open-circuit Voltage of Liquid Phase Crystallized Silicon Thin-film Solar Cells on Glass, J Photovolt 2015; 99:1-5.

[3] Dore J, Evans R, Schubert U, Eggleston BD, Ong D, Kim K, Huang J, Kunz O, Keevers M, Egan R, Varlamov S, and Green MA. Thin-film polycrystalline silicon solar cells formed by diode laser crystallisation, Prog Photovolt Res Appl 2013; 21, 6:1377–1383.

[4] Haschke J, Jogschies L, Amkreutz D, Korte L, and Rech B. Polycrystalline silicon heterojunction thin-film solar cells on glass exhibiting 582 mV open-circuit voltage, Sol Energy Mater Sol Cells 2013; 115:7–10.

[5] Masuko K, Shigematsu M, Hashiguchi T, Fujishima D, Kai M, Yoshimura N, Yamaguchi T, Ichihashi Y, Mishima T, Matsubara N, Yamanishi T, Takahama T, Taguchi M, Maruyama E, and Okamoto S. Achievement of More Than 25 % Conversion Efficiency With Crystalline Silicon Heterojunction Solar Cell, IEEE J Photovolt 2014; 4, 6:1433–1435.

[6] Nakamura J, Asano N, Hieda T, Okamoto C, Katayama H, and Nakamura K. Development of Heterojunction Back Contact Si Solar Cells, IEEE J Photovolt 2014; 4, 6:1491–1495.

[7] Dore J, Ong D, Varlamov S, Egan R, and Green MA. Progress in Laser-Crystallized Thin-Film Polycrystalline Silicon Solar Cells: Intermediate Layers, Light Trapping, and Metallization, IEEE J Photovolt 2014; 4, 1:33–39.

[8] Gabriel O, Frijnts T, Calnan S, Ring S, Kirner S, Opitz A, Rothert I, Rhein H, Zelt M, Bhatti K, Zollondz J, Heidelberg A, Haschke J, Amkreutz D, Gall S, Friedrich F, Stannowski B, Rech B, and Schlatmann R. PECVD Intermediate and Absorber Layers Applied in Liquid-Phase Crystallized Silicon Solar Cells on Glass Substrates, IEEE J Photovolt 2014; 4, 6:1343–1348.

[9] Amkreutz D, Haschke J, Häring T, Ruske F, and Rech B. Conversion efficiency and process stability improvement of electron beam crystallized thin film silicon solar cells on glass, Sol Energy Mater Sol Cells 2014; 123:13–16.

[10] Davis L. Properties of transparent conducting oxides deposited at room temperature, Thin Solid Films 1993; 236:1–2, 1–5.

[11] Hylton JD, Burgers AR, and Sinke WC. Alkaline Etching for Reflectance Reduction in Multicrystalline Silicon Solar Cells, J Electrochem Soc 2004; 151, 6: G408–G427.

[12] wafer ray tracer (version 1.4.3). http://www.pvlighthouse.com.au/ .